FATIGUE STRENGTH OF ANNEALED 0.37% CARBON STEEL CONTAINING SMALL DEFECT UNDER COMBINED AXIAL AND TORSIONAL LOADING

M. Endo*

Fatigue tests under combined axial and torsional in-phase loading conditions are carried out on annealed 0.37% carbon steel specimens containing an artificial small defect; either notch or hole. On the basis of observations of nonpropagating cracks emanating from defects, a model is given that, at fatigue limit, a defect in the combined stress state is equivalent to a mode-I crack having the same $\sqrt{area}$ and being normal to the maximum principal stress. Here, $\sqrt{area}$ is the geometrical parameter defined as the square root of the area of a defect or crack projected onto the plane of maximum principal stress. The fatigue limits obtained in the experiments for various defects and loading conditions are well predicted by the equation proposed in this study.

INTRODUCTION

For uniaxial fatigue, such as tension-compression or rotating-bending fatigue, it has been known that the fatigue strength of metals containing a small defect or crack is predicted by the following equations proposed by Murakami and Endo (1):

$$\Delta K_{th} = 3.3 \times 10^{-3} (H_V + 120) (\sqrt{area})^{1/3} \quad (1)$$

$$\sigma_w = 1.43 (H_V + 120) / (\sqrt{area})^{1/6} \quad (2)$$

where ΔK_{th} : stress intensity factor range (MPa$\sqrt{m}$), σ_w: fatigue limit stress amplitude (MPa), H_V : the Vickers hardness and $\sqrt{area}$: geometrical parameter (μm) which is defined as the square root of the projected area of a defect or crack.

The objective of this study is to discuss the application of this model, termed the $\sqrt{area}$ parameter model (2), to the multiaxial fatigue problem and finally propose an equation predicting the fatigue strength under combined axial/torsional loading.

* Dept. of Mechanical Engineering, Fukuoka University, Fukuoka 814-0180, Japan.

MATERIAL AND EXPERIMENTAL PROCEDURE

The material used is an annealed 0.37% carbon steel. The chemical composition (wt.%) is: 0.37C, 0.21Si, 0.65Mn, 0.019P, 0.017S, 0.13Cu, 0.06Ni, 0.14Cr. The tensile strength is 586MPa, the reduction in area is 50.7% and the Vickers hardness is 160. The geometry of smooth specimen is shown in Fig. 1. The defect specimen has a small defect artificially machined on the surface. The geometries of defects are shown in Fig. 2. All specimens were electropolished before fatigue testing.

For combined and torsional loading tests, a hydraulic axial/torsional fatigue testing machine was used operating at 30Hz. Uniaxial loading tests were carried out either on a hydraulic uniaxial fatigue testing machine with the operating speed 50Hz or a rotating-bending testing machine of the uniform moment type, with the operating speed 57Hz. All tests were performed under the loading conditions of in-phase tension-compression and reversed torsion (R = -1). The loading ratios of axial to torsional stress amplitude were τ/σ = 0, 1/2, 1, 2 and ∞.

The fatigue limits τ_{cw} and σ_{cw} under the combined loading are defined as the maximum nominal stresses under which a specimen endured 10^7 cycles at a constant loading ratio τ/σ. The minimum step of stress level was σ = 5MPa when $\tau/\sigma \leq 1$ and τ = 5MPa when $\tau/\sigma \geq 1$.

EXPERIMENTAL RESULTS AND DISCUSSION

Fatigue Limit of Smooth Specimen and Non-detrimental Defect

The fatigue limit of smooth specimen obtained in the tension-compression test (230MPa) was almost equal to that obtained in the rotating-bending test (235MPa), and the influence of stress gradient is considered to be small. The ratio of the rotating-bending fatigue limit (235MPa) to the torsional fatigue limit (145MPa) was 0.62.

Reducing the defect size below a critical size, the fatigue strength of defect specimen was equal to that of smooth specimen. The critical size of defect which does not influence the fatigue strength increased with τ/σ. For example, a circumferential notch of 10μm depth lowered about 9% the fatigue strength under the uniaxial loading (τ/σ = 0), while under τ/σ = 1 the same notch was non-detrimental.

Modeling of Fatigue Limit of Defect Specimen under Combined Stress

Figure 3 shows the nonpropagating cracks observed at the fatigue limits of notched and holed specimens. In the case of holed specimens, the direction of

nonpropagating crack emanating from a hole was approximately normal to the principal stress σ_1. On the surface of notch root, many cracks initiated along the plane of maximum shear stress, then many of them bent or branched to propagate approximately in the direction normal to σ_1 and finally ceased propagation. Under a stress slightly higher than the fatigue limit, a crack propagating in the direction normal to σ_1 leaded the specimen to break.

The above observational results suggest that the fatigue limit of defect specimens is determined by the threshold condition for propagation of a mode I crack (stage II crack). This makes one to expect that the $\sqrt{area}$ parameter model, whose usefulness has been confirmed in the uniaxial fatigue problems (1)(2), could be applied to the fatigue strength problem of defect specimens under combined stress. As shown in Fig. 4, therefore, it is modeled in this study that the problem is equivalent to the fatigue threshold problem of a small mode-I crack having the same $\sqrt{area}$ and being normal to the maximum principal stress σ_1. Here, $\sqrt{area}$ is redefined as the square root of the area obtained by projecting a defect onto the plane of maximum principal stress. The values of $\sqrt{area}$ for defects used in this work are given by the equations in Fig. 2; see references (1) and (2).

Factors Affecting the Threshold Stress Intensity Factor Range

In Fig. 4, the maximum value of mode I stress intensity factor $K_{I\max}$ along the crack front is calculated by the following equation obtained by elastic analysis (1).

$$K_{I\max} \cong 0.650\, \sigma_1 \sqrt{\pi\sqrt{area}} \tag{3}$$

The experimental values of the threshold stress intensity factor range $\Delta K_{th,exp}$ of defect specimens are calculated using Eq.(3) from the principal stress range at fatigue limit and $\sqrt{area}$ of a defect. Figure 5 shows the relationship between $\Delta K_{th,exp}$ and $\sqrt{area}$. The line in this figure, predicted by Eq.(1), shows a good agreement with the uniaxial results ($\tau/\sigma = 0$). Other results also show the same dependence of $\Delta K_{th,exp}$ on $\sqrt{area}$, but they are lower than the uniaxial results.

According to the studies on the effect of biaxial stress on the fatigue crack propagation behaviour at zero mean load (R=-1) (Hopper and Miller (3), Kitagawa et al (4), Harada et al. (5) and McClung (6)), the effect of stress biaxiality increases with increasing the stress level and with decreasing the crack length, and the compressive stress parallel to the crack accelerates the propagation. Figure 6 shows the dependence of $\Delta K_{th,exp}$ on the stress biaxiality. In this figure, the ordinate is the value of $\Delta K_{th,exp}$ normalized by ΔK_{th}, which is predicted for uniaxial case ($\tau/\sigma = 0$) by Eq.(1), and the abscissa is the principal stress amplitude ratio $\lambda = \sigma_2/\sigma_1$. In spite of

the large difference in defect shape, size and orientation, the effect of defects is expressed only by a single geometrical parameter, $\sqrt{area}$. though a dependence of $\Delta K_{th,exp}$ on λ is observed. By representing this trend by a straight line shown in Fig. 6, we obtain the following equation.

$$\Delta K_{th,exp} = [(1 - \phi)\lambda + 1]\Delta K_{th} \quad ; \phi = 0.86 \tag{4}$$

Prediction of Fatigue Limit

For a given combination of H_V, $\sqrt{area}$ and λ, fatigue limits, τ_{cw} and σ_{cw}, are predicted from Eqs.(1), (3) and (4). Figure 7 shows the comparison of the predicted values with the experimental results. The values of τ_{cw} and σ_{cw} on the both axes are normalized by the uniaxial fatigue limit σ_w predicted by Eq.(2). The experimental results obtained for various defects and loading conditions are well predicted. In this figure, a curve representing the following Findley (7) type equation is also shown.

$$\sigma_{cw}/\sigma_w + (\tau_{cw}/\phi\sigma_w)^2 = 1 \qquad ; \phi = 0.86 \tag{5}$$

The difference between two curves is small. Prediction by Eq.(5) is rather useful than Eq.(4) because of the easer calculation. In Eq.(5), σ_w is predicted by Eq.(2) from a material parameter, H_V, and a geometrical parameter of a defect, $\sqrt{area}$.

ACKNOWLEDGEMENTS

This work has been supported by the Fukuoka Industry, Science & Technology Foundation, Fukuoka, Japan.

REFERENCES

(1) Murakami, Y. and Endo, M., *The Behaviour of Short Fatigue Cracks*, Edited by K. J. Miller and E. R. de los Rios, Mech. Engng. Publ., London, 1986, pp.275-293.
(2) Murakami, Y. and Endo, M., *Theoretical Concepts and Numerical Analysis of Fatigue*, Edited by A. F. Blom and C. J. Beevers, Engng. Mater. Advisory Services Ltd., London, 1992, pp.51-71.
(3) Hopper, C. D. and Miller, K. J., J. *Strain Analysis*, Vol.12, No.1, 1977, pp.23-28
(4) Kitagawa, H. et al., *Multiaxial Fatigue, ASTM STP 853*, Edited by K. J. Miller and M. W. Brown, ASTM, Philadelphia, 1985, pp.164-183.
(5) Harada, S at al., *J. Soc. Mater. Sci., Japan*, Vol.36, No.401, 1987, pp.147-152.
(6) McClung, R. C., *Fatigue Fract. Engng. Mater. Struct.*, Vol.12, No.5, 1989, pp.441-460.
(7) Findley, W. N., *Trans. ASME*, Vol.79, 1957, pp.1337-1348.

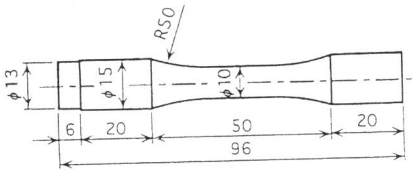

Figure 1 Smooth specimen geometry; dimensions in millimeters.

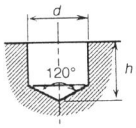

(a) Drilled hole; $d = h = 100$ and $500\mu m$, $\sqrt{area} = \sqrt{d[h-d/(4\sqrt{3})]}$

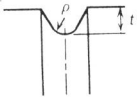

(b) Circumferential notch; ρ = 10 - 50μm, t = 10 - 200μm, $\sqrt{area} = \sqrt{10}\,t$

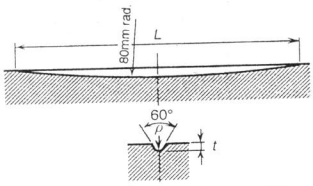

(c) Longitudinal notch; ρ = 50μm, t = 100μm, $\sqrt{area} = \sqrt{10}\,t$.

Figure 2 Shapes and dimensions of defects.

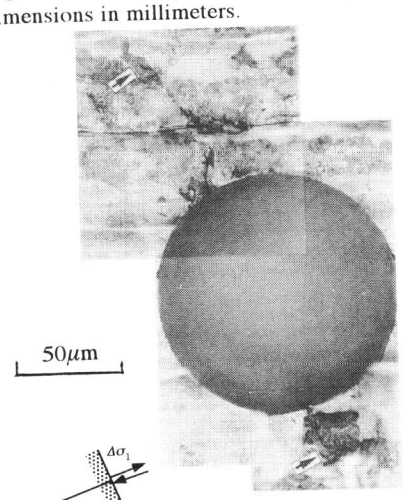

(a) τ_{cw}/σ_{cw}=1/2 (τ_{cw}=72.5MPa, σ_{cw}=145MPa), Hole: d=h=100μm.

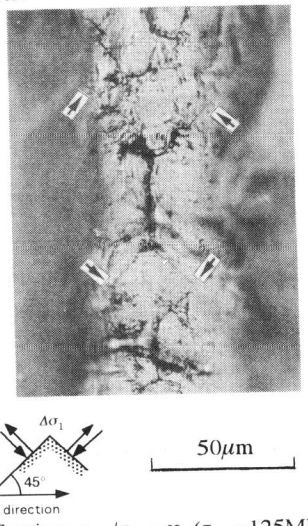

(b) Torsion: $\tau_{cw}/\sigma_{cw}=\infty$ (τ_{cw}=125MPa, σ_{cw}=0), Notch: ρ=50μm, t=200μm.

Figure 3 Nonpropagating cracks observed at fatigue limit.

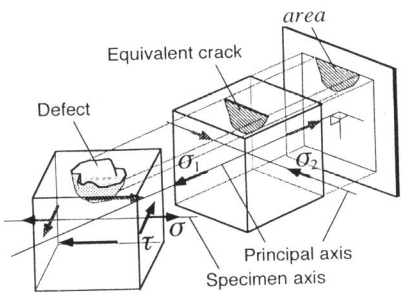

Figure 4 Defect and the equivalent crack.

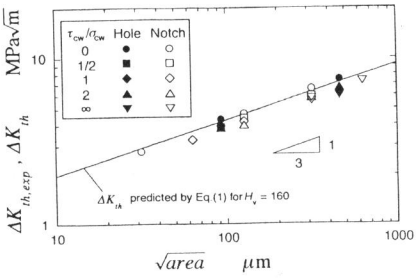

Figure 5 Relationship between $\Delta K_{\mathrm{th,exp}}$ and $\sqrt{area}$.

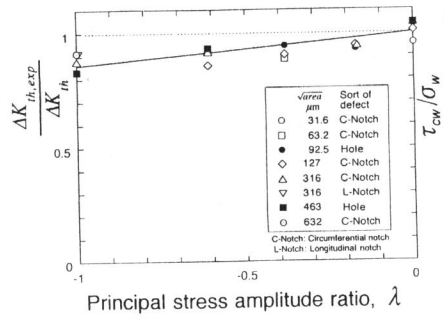

Figure 6 Dependence of $\Delta K_{\mathrm{th,exp}}$ on stress biaxiality.

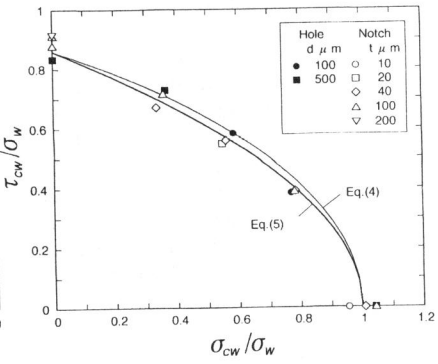

Figure 7 Relationship between $\tau_{\mathrm{cw}} / \sigma_{\mathrm{w}}$ and $\sigma_{\mathrm{cw}} / \sigma_{\mathrm{w}}$.